Electrokinetically induced alterations in dynamic response of viscoelastic fluids in narrow confinements

Aditya Bandopadhyay and Suman Chakraborty
Department of Mechanical Engineering, IIT Kharagpur, Kharagpur 721302, India
(Received 18 January 2012; revised manuscript received 20 March 2012; published 7 May 2012)

We investigate a dynamical interplay between interfacial electrokinetics and a combined dissipative and elastic behavior of flow through narrow confinements, in analogy with spatiotemporal hydrodynamics of porous media. In particular, we investigate the effects of streaming potential on the pertinent dynamic responses, by choosing a Maxwell fluid model for representing the consequent electro-hydrodynamic characteristics. We transform the pertinent governing equation to the frequency domain, so that a dynamic generalization of Darcy's law in the presence of streaming potential effects can be effectively realized. We show that the frequencies corresponding to local maxima in the dynamic permeability also correspond to local maxima in the induced streaming potential. We also bring out the effects of Stern layer conductivity on the dynamic permeability. Our analytical estimates do reveal that serious overestimations in the commonly portrayed notion of massive amplifications of dynamic permeability at resonating frequencies may be possible, if interactions between spontaneous electrochemical interfacial phenomena and pulsating pressure-gradient-driven viscoelastic transport are trivially ignored.

DOI: 10.1103/PhysRevE.85.056302 PACS number(s): 47.61.−k

I. INTRODUCTION

Many physical problems involve the response of a fluid against an applied frequency-dependent pressure gradient. An elegant way of characterizing such frequency-dependent processes, in analogy with flow through porous media, may be realized through a frequency-dependent permeability function, also known as dynamic permeability [1–4], which in essence is a permeability parameter associated with a dynamic generalization of Darcy's law in a transformed frequency domain. Based on the consideration of this function, it has been reported in the literature that by exploiting a complicated interplay of the effects of elasticity and dynamically evolving dissipative characteristics of a viscoelastic fluid, it may be possible to realize dramatic enhancements in the dynamic permeability at certain frequencies [1–12], bearing far-ranging consequences both from scientific as well as technological perspectives. While arriving at the above inferences on "dramatic" enhancement in the dynamic responses of a viscoelastic fluid flowing through a conduit, however, any possibilities of intricate interactions between interfacial electromechanics and response of a fluid to a frequency-dependent pressure gradient have grossly been ignored. In reality, on the other hand, small-scale fluidic pathways are often faceted by the formation of a charged layer adhering to the substrate walls, eventually giving rise to the formation of an electrical double layer (EDL). Fundamentally, the EDL [13–16] refers to two parallel layers of charge surrounding a solid substrate. The first layer consists of surface charges that are directly adsorbed on the solid substrate. The second layer involves ions that are attracted to the surface charge via Coulombic interactions, electrically screening the first layer. This second layer, also known as the diffuse part of the EDL, is composed of mobile ions that are subjected to the combined influences of electrostatic and thermal interactions. As a consequence of EDL formation, there occurs a preferential release of counterions (i.e., ions bearing charges opposite in sign to that of the surface charges) to the interfacial fluid, consistent with the competing effects of Coulombic and entropic interactions. Notably, these effects may spontaneously manifest even in the absence of any external electrical field. Further, in the presence of a driving pressure gradient, the excess counterions in the EDL may get advected to the downstream end of the fluidic confinement. This, in turn, induces a back electrical potential, also known as streaming potential [13,14], which tends to oppose the pressure-driven fluidic transport, i.e., the very cause to which it is due. As a consequence, there appears to be an enhanced resistance against fluid motion, which is traditionally known as the electroviscous effect. Such electroviscous effects may bear several nontrivial implications, in particular, for cases in which the characteristic constitutive behavior of the fluid deviates from Newtonian characteristics.

A wide gamut of literature has been reported on electrokinetic interactions involving non-Newtonian fluids in narrow confinements [17–32]. Afonso *et al*. [17] have derived analytical solutions for combined electro-osmotic and pressure-driven flows of viscoelastic fluids in microchannels. For their analysis, they have considered the Phan-Thien Tanner (PTT) and finitely extensible nonlinear elastic and Peterlin (FENE-P) models. Berli *et al*. [18] have addressed the issue of wall-adjacent depletion layers occurring in the flows of non-Newtonian fluids, especially those involving macromolecules such as polymer solutions. They have derived and shown the validity of Onsager force-flux relations, under these conditions. Das and Chakraborty [19] have derived analytical solutions for the electro-osmotic transport of non-Newtonian fluids in rectangular microchannels, and have presented a case study for the transport of blood in which the relative size of the channel width to the red blood cell (RBC) plays a crucial role toward dictating the flow characteristics. Dhinakaran *et al*. [20] have investigated the electro-osmotic flows for viscoelastic fluids considering the PTT model, taking the nonlinearity of the Poisson-Boltzmann equation aptly into account. Graham and Jones [21] have discussed the behavior of spherical particles in a flow of power-law fluids. Hadigol *et al*. [22] have numerically obtained the pressure rise due to the electro-osmotic flow of power-law fluids in slit channels. Olivares *et al*. [23] have investigated the flow of polymer solutions by considering the effect of wall depletion. Park and Lee [24] have discussed the

flow of viscoelastic fluids in straight microchannels and have shown the presence of secondary flows for the pressure-driven transport of viscoelastic fluids and the effect of an enhanced volume flow rate on the dispersion of the solutes. Vasu and De [25] have discussed the electroviscous effects for the flow of power-law fluids in slit microchannels. Zhao and Yang [26] have derived analytical solutions for the Smoluchowski velocity in the case of arbitrary surface potential. In their work, Zhao and Yang [27] have considered the flow of power-law fluids in microchannels in the presence of electrokinetic effects. Zhao *et al*. [28] have discussed the mathematical derivation for electro-osmotic velocity fields of viscoelastic fluids in rectangular microchannels. Zimmerman *et al*. [29] have numerically solved for the electro-osmotic flow of Carreau fluids in the T junction of a microchannel, by making use of a simplified slip model at the wall. Tang *et al*. [30] have used lattice Boltzmann simulations to solve for the potential and velocity distribution in electro-osmotically driven flow fields of power-law fluids. Akgul and Pakdemirli [31] have compared the approximate and numerical solutions of velocity fields corresponding to electro-osmotic flows of third grade fluids in microparallel plates. Zhao and Yang [32] have derived analytical solutions for the electro-osmotic velocity profiles of Oldroyd-B-type fluid and have extended their analysis to special cases of Newtonian fluid and second grade fluid. However, a common consensus that can be arrived at from the literature reported above is that any kind of interconnection between interfacial electromechanics and possibilities in giant amplifications of dynamic permeabilities of viscoelastic fluids in narrow confinements has so far been grossly overlooked.

In the present study, we investigate the implications of streaming potential toward altering dynamic permeabilities of Maxwell fluids in narrow confinements subjected to interfacial electromechanical interactions. The concerned analysis is essentially centered around a competition between dissipative, electrokinetic, and elastic effects. Our studies do reveal that frequencies corresponding to local maxima in the dynamic permeabilities also corroborate corresponding local maxima in the streaming potential. Accordingly, any phenomenal enhancements in the dynamical response at such resonating frequencies, as postulated in earlier reported literature, may tend to get arrested to a significant extent. Following this up, our results infer that serious overestimations with regard to predictions on augmentations in the dynamic permeability may be incurred, in case interfacial electrokinetic interactions are not aptly taken into consideration, disregarding the absence of any external electrical field. We also delineate the role of Stern layer (effectively, an immobilized ionic layer at the fluid-solid interface) conductivity on the underlying electrohydrodynamic mechanisms.

II. FREQUENCY-DEPENDENT PERMEABILITY IN THE PRESENCE OF STREAMING POTENTIAL EFFECTS

We consider the flow of a linearized Maxwell fluid often considered to mimic common biophysical fluids such as blood (for example, see Refs. [33,34]) in a parallel plate microchannel configuration (with channel height of $2H$), subjected to an oscillatory driving pressure gradient, but without the application of any external electric field. An electrical field, however, is spontaneously induced, as attributable to intricate electromechanical interactions in the narrow confinement. A comprehensive assessment of the electrical potential distribution in the EDL is central to the understanding of the concerned fluid dynamic implications. Hence, we first briefly describe the pertinent EDL phenomenon.

A. Potential distribution within the EDL

The potential distribution (ψ) in the EDL is coupled with the charge density distribution (ρ_e) in the same through the Poisson equation, as given by Refs. [13,14]

$$\nabla^2\psi = -\rho_e/\varepsilon, \tag{1a}$$

where

$$\rho_e = e(z^+n^+ + z^-n^-). \tag{1b}$$

Here e is the protonic charge, z^+ and z^- represent the valency of positively and negatively charged species, respectively; n^+ and n^- represent the ionic number densities of the positive and negative species, respectively. Under nonoverlapped EDL conditions, negligible ionic advection as compared to ionic diffusion in the wall-transverse direction, and idealization of the ionic species as point charges, the ionic number densities can be expressed by the Boltzmann distribution, which is given as [13,14]

$$n_\pm = n_0 \exp(-z_\pm e\psi/k_BT). \tag{2}$$

The substitution of Eqs. (1b) and (2) in Eq. (1a) leads to the following equation describing the potential distribution in the EDL for a z:z symmetric electrolyte:

$$\frac{d^2\psi}{dy^2} = \frac{2zen_0}{\varepsilon}\sinh\left(\frac{ze\psi}{K_BT}\right), \tag{3}$$

where y is the coordinate direction normal to the confining boundaries, and $\lambda = \sqrt{\varepsilon k_BT/2z^2e^2n_0}$ is a characteristic length scale of the EDL (also known as Debye length); the bulk ionic number concentration being taken as n_0. Equation (3) is subject to the following boundary conditions: at $y = 0$, $\psi = \zeta$ (zeta potential) and at $y = H$, $d\psi/dy = 0$. Equation (3) can be solved analytically to yield the following EDL potential description:

$$\bar{\psi} = \frac{4}{\bar{\zeta}}\tanh^{-1}\left[\tanh\left(\frac{\bar{\zeta}}{4}\right)\exp\left(\frac{-\bar{y}}{\lambda/H}\right)\right] \quad \text{for} \quad 0 \leqslant \bar{y} \leqslant 1, \tag{4a}$$

where $\bar{\psi} = \psi/\zeta, \bar{\zeta} = ze\zeta/K_BT$, and $\bar{y} = y/H$. There are several subtle and interesting issues that lead toward the derivation of the above solution (for details, see Refs. [13,35–40]). Important considerations concerning the above are provided in the form of Appendix A in our paper, for the sake of completeness.

As a further simplification, for "low" zeta potentials (typically <25 mV in magnitude, in practice), Eq. (4a) can be linearized (classically known as Debye-Hückel linearization; see Ref. [13]) to get a simpler solution of the form of:

$$\bar{\psi} = \frac{\cosh\left(\frac{\bar{y}-1}{\lambda/H}\right)}{\cosh\left(\frac{H}{\lambda}\right)}. \tag{4b}$$

B. Fluid dynamics and dynamic permeability

We consider flow in the geometry defined previously. The pertinent equation of motion is the momentum equation (5), which considers the effect of the added body force due to the induced streaming potential field, *despite no application of any external electrical field*, as [41–49]

$$\rho\frac{\partial \mathbf{v}}{\partial t} = -\nabla p + \nabla\cdot\boldsymbol{\tau} + \rho_e\mathbf{E}. \tag{5}$$

Here ρ is the fluid density, $\mathbf{v}$ is the fluid velocity vector, ρ_e is the net ionic charge density, p represents the pressure, $\mathbf{E}$ is the induced electric field due to streaming potential effects, and $\boldsymbol{\tau}$ is the viscous stress tensor. It is important to mention in this context that the aim here has been to study an unsteady flow field subjected to an oscillatory forcing mechanism, under the situation that convective terms in the Navier Stokes equation can be neglected, based on the considerations of an unidirectional and incompressible flow (so that $\partial u/\partial x = 0$ and $v = 0$); for details, please see Ref. [50]. This consideration is similar to that involved in solving the Stokes second problem in classical fluid mechanics, in which only the temporal component of the acceleration is considered (for example, see Refs. [4,36,45]). Such analysis is common in cases in which the forcing function is periodic in nature and the flow has reached a fully developed steady state, which leads to a natural dropping of the convective acceleration terms.

For representing the viscoelastic behavior, we make use of the linear form of the Maxwell model, given as [51]

$$t_m\frac{\partial \boldsymbol{\tau}}{\partial t} = \eta\nabla\mathbf{v} - \boldsymbol{\tau}, \tag{6}$$

where t_m represents the relaxation time, and η is the viscosity. This model shows Newtonian behavior in the limiting case as the relaxation time tends to 0.

We proceed to solve the scalar component of Eq. (5) along the axial (X) direction, by substituting Eq. (6) in Eq. (5), substituting ρ_e from Eq. (1b), and making use of the solution for ψ [Eq. (4)], to get

$$\rho\frac{\partial u}{\partial t} = -\frac{\partial p}{\partial x} + \eta\nabla^2 u - t_m\rho\frac{\partial^2 u}{\partial t^2} - t_m\frac{\partial}{\partial t}\left(\frac{\partial p}{\partial x}\right) + t_m\rho_e\frac{\partial E}{\partial t} + \rho_e E. \tag{7}$$

Taking Fourier transform of Eq. (7), we get

$$\frac{d^2U}{dy^2} + U\left(\frac{i\rho\omega + \rho\omega^2 t_m}{\eta}\right) = \frac{1}{\eta}\frac{\partial P}{\partial x}(1 - i\omega t_m) + \frac{\varepsilon\tilde{E}}{\eta}\frac{d^2\psi}{dy^2}(1 - i\omega t_m). \tag{8}$$

Equation (8) is subjected to the following boundary conditions: $y = 0$, $U = 0$ (no slip); $y = H$, $dU/dy = 0$ (symmetry). In Eq. (8), U, P, and $\tilde{E}$ represent the respective transformed quantities.

For representing the solution of Eq. (8) in a normalized form, we consider the following dimensionless parameters: $\bar{y} = y/H$, $\omega^* = \omega t_m$, $\beta^2 = \rho(\omega^{*2} + i\omega^*)/\eta t_m$, $U^* = U/[(\partial P/\partial x)H^2/\eta]$, $\bar{E} = \tilde{E}/[(\partial P/\partial x)H^2/\varepsilon\zeta]$, $\bar{\omega} = i\omega t_m + \omega^2 t_m^2$, and $\alpha = \rho H^2/\eta t_m$. The dimensionless parameter α can be identified as the inverse of the Deborah number [4], which is the ratio of the viscous time scale ($t_v = \rho H^2/\eta$) to the relaxation time (t_m). Based on these normalization parameters, the transformed dimensionless velocity field, in a compact analytical form, may be described as

$$\begin{aligned} U^* = {} & \left(\frac{1 - i\omega^*}{\alpha\bar{\omega}}\right)\left(1 - \frac{\cos[\sqrt{\alpha\bar{\omega}}(1-\bar{y})]}{\cos(\sqrt{\alpha\bar{\omega}}H)}\right) + \bar{E}\frac{1 - i\omega^*}{\bar{\zeta}\left(\frac{\lambda}{H}\right)^2\sqrt{\alpha\bar{\omega}}}\Bigg[-\cos(\sqrt{\alpha\bar{\omega}}\bar{y})\int_0^{\bar{y}}\sinh(\bar{\psi}\bar{\zeta})\sin(\sqrt{\alpha\bar{\omega}}\bar{y})d\bar{y} \\ & + \sin(\sqrt{\alpha\bar{\omega}}\bar{y})\int_0^{\bar{y}}\sinh(\bar{\psi}\bar{\zeta})\cos(\sqrt{\alpha\bar{\omega}}\bar{y})d\bar{y} - \sin(\sqrt{\alpha\bar{\omega}}\bar{y})\tan(\sqrt{\alpha\bar{\omega}})\int_0^{1}\sinh(\bar{\psi}\bar{\zeta})\sin(\sqrt{\alpha\bar{\omega}}\bar{y})d\bar{y} \\ & - \sin(\sqrt{\alpha\bar{\omega}}\bar{y})\int_0^{1}\sinh(\bar{\psi}\bar{\zeta})\cos(\sqrt{\alpha\bar{\omega}}\bar{y})d\bar{y}\Bigg]. \end{aligned} \tag{9a}$$

For details of obtaining the above solution, please refer to Appendix B. Equation (9a) can be further simplified using the Debye-Hückel linearization, to yield

$$U^* = \left(\frac{1 - i\omega^*}{\alpha\bar{\omega}}\right)\left(1 - \frac{\cos[\sqrt{\alpha\bar{\omega}}(1-\bar{y})]}{\cos(\sqrt{\alpha\bar{\omega}}\bar{y})}\right) + \frac{\bar{E}(1 - i\omega^*)}{[1 + \alpha\bar{\omega}(\lambda/H)^2]}\left(\frac{\cosh\left(\frac{\bar{y}-1}{\lambda/H}\right)}{\cosh\left(\frac{H}{\lambda}\right)} - \frac{\cos[\sqrt{\alpha\bar{\omega}}(\bar{y}-1)]}{\cos(\sqrt{\alpha\bar{\omega}})}\right). \tag{9b}$$

The dynamic permeability is traditionally defined as $\langle U\rangle = -K(\omega)\left[(\partial P/\partial x)/\eta\right]$. Further, we can define a nondimensional dynamic permeability as $K^* = -K/H^2$, so that $\langle U^*\rangle = K^*$. Thus, the dimensionless dynamic permeability can be found out by taking a spatial average of the velocity obtained from Eq. (9a) or (9b).

It is important to mention here that Eqs. (9a) and (9b) are not yet mathematically closed, since the streaming potential appears to be a yet undetermined parameter, which in turn strongly depends on the velocity field itself. The pertinent closure relationship is provided by an overall electroneutrality constraint, as described subsequently.

C. Overall electroneutrality constraint

Since there is no externally applied electric field, the streaming current (due to the net advection of ions) must be counterbalanced by the net conduction (electromigration) current over each channel section, so as to preserve electroneutrality, i.e., net zero current in the channel at any instant. The net current, in turn, can be written as

$$I_{\text{net}} = I_{\text{stream}} + I_{\text{cond}} + I_{\text{Du}} = 0, \tag{10}$$

where $I_{\text{stream}} = \int_0^H ze(n^+ - n^-)u\,dy$ is the streaming current, $I_{\text{cond}} = \int_0^H (z^2e^2E/f)(n^+ + n^-)dy$ is the conduction current through the "mobile" fluid layers, and $I_{\text{Du}} = \sigma_{\text{st}}E$ is the conduction current through the "immobilized" Stern layer; f being the ionic friction coefficient (assumed to be the same for the cationic and anionic species, for simplicity). Normalized with respect to a reference streaming current $I_{s,\text{ref}} = -2z^2e^2n_0U_{\text{ref}}H\zeta/K_BT$, the electroneutrality condition given by Eq. (10) essentially implicates

$$\int_0^1 U^* \frac{\sinh(\bar{\psi}\bar{\zeta})}{\bar{\zeta}} d\bar{y} + J\bar{E}\int_0^1 \cosh(\bar{\zeta}\bar{\psi})d\bar{y} + J\,\text{Du}\,\bar{E} = 0, \tag{11}$$

where $J = I_{c,\text{ref}}/I_{s,\text{ref}}$ and $I_{c,\text{ref}} = 2z^2e^2E_{\text{ref}}n_0Hf$. Here $E_{\text{ref}} = U_{\text{ref}}\eta/\varepsilon\zeta$ and the Dukhin number is defined as $\text{Du} = \sigma_{\text{st}}/H\sigma_{\text{bulk}}$, where $\sigma_{\text{bulk}} = 2n_0z^2e^2/f$ is the bulk ionic conductivity. Thus, from Eq. (11) we get

$$I_1 + \bar{E}I_2 + JI_3\bar{E} + J\,\text{Du}\,\bar{E} = 0. \tag{12}$$

The various integrals appearing in Eq. (12) are given by

$$I_1 = \int_0^1 \left(\frac{1 - i\omega^*}{\alpha\bar{\omega}}\right)\left(1 - \frac{\cos[\sqrt{\alpha\bar{\omega}}(1-\bar{y})]}{\cos(\sqrt{\alpha\bar{\omega}})}\right)\frac{\sinh(\bar{\psi}\bar{\zeta})}{\bar{\zeta}}d\bar{y},$$

$$I_2 = \frac{1 - i\omega^*}{\bar{\zeta}^2\left(\frac{\lambda}{H}\right)^2\sqrt{\alpha\bar{\omega}}}\int_0^1 \Bigg[-\cos(\sqrt{\alpha\bar{\omega}}\bar{y})\int_0^{\bar{y}} \sinh(\bar{\psi}\bar{\zeta})\sin(\sqrt{\alpha\bar{\omega}}\bar{y})d\bar{y} + \sin(\sqrt{\alpha\bar{\omega}}\bar{y})\int_0^{\bar{y}} \sinh(\bar{\psi}\bar{\zeta})\cos(\sqrt{\alpha\bar{\omega}}\bar{y})d\bar{y}$$
$$- \sin(\sqrt{\alpha\bar{\omega}}\bar{y})\tan(\sqrt{\alpha\bar{\omega}})\int_0^1 \sinh(\bar{\psi}\bar{\zeta})\sin(\sqrt{\alpha\bar{\omega}}\bar{y})d\bar{y} - \sin(\sqrt{\alpha\bar{\omega}}\bar{y})\int_0^1 \sinh(\bar{\psi}\bar{\zeta})\cos(\sqrt{\alpha\bar{\omega}}\bar{y})d\bar{y}\Bigg]\frac{\sinh(\bar{\psi}\bar{\zeta})}{\bar{\zeta}}d\bar{y}.$$

Upon linearization, the above integrals can be simplified as

$$I_1 = \int_0^1 \left(\frac{1 - i\omega^*}{\alpha\bar{\omega}}\right)\left(1 - \frac{\cos[\sqrt{\alpha\bar{\omega}}(1-\bar{y})]}{\cos(\sqrt{\alpha\bar{\omega}})}\right)\bar{\psi}\,d\bar{y},$$

$$I_2 = \int_0^1 \frac{(1 - i\omega^*)}{[1 + \alpha\bar{\omega}(\lambda/H)^2]}\left(\frac{\cosh\left(\frac{\bar{y}-1}{\lambda/H}\right)}{\cosh\left(\frac{H}{\lambda}\right)} - \frac{\cos[\sqrt{\alpha\bar{\omega}}(\bar{y}-1)]}{\cos(\sqrt{\alpha\bar{\omega}})}\right)\bar{\psi}\,d\bar{y},$$

whereas

$$I_3 = \int_0^1 \cosh(\bar{\zeta}\bar{\psi})d\bar{y}.$$

From Eq. (12) we get

$$\bar{E} = \frac{-I_1}{I_2 + J\,(I_3 + \text{Du})}. \tag{13}$$

In the form of Eq. (13), we have obtained an expression for the streaming potential by making use of the electroneutrality criterion, which can act as a necessary closure to the present formalism. Equation (13) can now be substituted in Eq. (9a) or (9b) to find the velocity profile, so as to obtain the dynamic permeability.

III. RESULTS AND DISCUSSIONS

At this stage, it is imperative to reiterate that a focal theme of the present work is to bring out the implications of interfacial electrokinetics toward altering the dynamic response of viscoelastic fluids in narrow confinements. Toward assessing the underlying consequences, it may be appropriate if we first look into the characteristic responses in terms of the streaming potential development in the frequency domain, as a function of relevant controlling parameters. In an effort to embed elements of practicality into the corresponding physical features, we consider the flow of human blood sample, for which $\rho \sim 10^3$ kg m^{-3}, $\eta = 10^{-3}$–10^{-2} Pa s (for shear rate in the region of $\sim 10^2$–10^3 s^{-1} with hematocrit $\sim$30% at 18 °C) and $H \sim 10^{-6}$ m, $t_m \sim 10^{-2}$ s [4] so that $\alpha \sim 10^{-4}$, which is a typical inverse Deborah number for most biofluids. To cover a wider range of fluids, we further consider $t_m \sim 10^{-2}$ s to 10^{-4} s, which lead to $\alpha \sim 10^{-2}$ to 10^{-4}. Further, we take the dimensionless parameter J [please refer to its definition in the discussion following Eq. (11)], which represents the ratio of the characteristic estimates of conduction current and streaming current, to be -10, considering ionic diameter $\sim$1 Å, $\zeta = -25$ mV, and a valency of 1. We also consider the Dukhin number to vary from 0 to 10 [52], considering reported data. We characterize the deviation from classical Newtonian behavior by invoking the Deborah number. As the relaxation time tends to 0, one approaches the classical Newtonian behavior. Thus, small relaxation times are fair indicators of small perturbation of the fluid characteristics from Newtonian behavior. Smaller inverse

Deborah numbers, interestingly, are implicators of larger relaxation times, signifying large deviations from Newtonian behavior.

Figure 1(a) depicts the variation of the dimensionless induced streaming potential field ($\bar{E}$) as a function of dimensionless frequency (ω^*) for different inverse Deborah numbers. We observe that for lower values of α, the magnitude of the streaming potential at the resonant frequency increases. Also, the dimensionless frequency at which the resonance occurs increases with decreasing value of α. Importantly, characteristics mimicking close-to-Newtonian behavior are manifested in terms of small relaxation times, implicating large values of α. It can be clearly seen that when the fluid is Newtonian, the behavior is dissipative for all frequencies. Since the dissipative behavior of the system is more prominently manifested as the value of α increases, the corresponding streaming current (essentially an advective current of ions) at resonating frequency also weakens. This in turn leads to a reduced conduction current, which in turn is reflected by the reduced induced streaming potential field.

Figure 1(b) depicts the variation of dimensionless streaming potential field ($\bar{E}$) as a function of the dimensionless frequency (ω^*), for different Dukhin numbers (Du). Physically, the Dukhin number is a measure of the ratio of the Stern layer conductivity to the bulk conductivity. Hence, a larger Dukhin number would indicate larger Stern layer conductivity as compared to that of the bulk fluid [52], in which case the conduction current through the Stern layer would be more proportionately enhanced than that through the bulk fluid. The presence of the Stern layer, therefore, in effect, leads to a decreased $\bar{E}$ because of the fact that as the conductance increases, the required electric potential necessary to balance out the streaming current decreases. Larger Stern layer conductivity, accordingly, would lead to a decreased amount of conduction current through the bulk. Bulk conduction current is in a direction opposite to the flow and hence leads to enhanced effective viscous resistances. When the conduction current in the bulk decreases (may be attributed to large electrical conductivities of the Stern layer), the electroviscous resistance decreases and hence the flow behaves as if there are no streaming potential effects. As a consequence, as the Dukhin number increases, the magnitude of $\bar{E}$ decreases. Interestingly, the resonant frequency appears to be higher for lower values of the Dukhin number. This may be attributed to the fact that a lack of stern layer conductivity leads to a larger induced electric field, which in turn increases the contribution of the electrical term to the velocity field, implicating a larger damping term in the elastic system and hence a shift toward larger resonant frequency.

Figure 1(c) depicts the variation of dimensionless streaming potential field ($\bar{E}$) as a function of the dimensionless frequency (ω^*), for different channel width to Debye length ratios (H/λ). A larger value of H/λ is representative of the fact that the channel width is much larger than the characteristic EDL thickness. This, in effect, would signify decreased contributions from the EDL toward dictating the bulk advective transport of surplus counterions, considering the fact that the EDL effects remain essentially confined in a region in close proximity of the channel walls. Thus, larger H/λ values would imply weakened strengths of the induced streaming potential

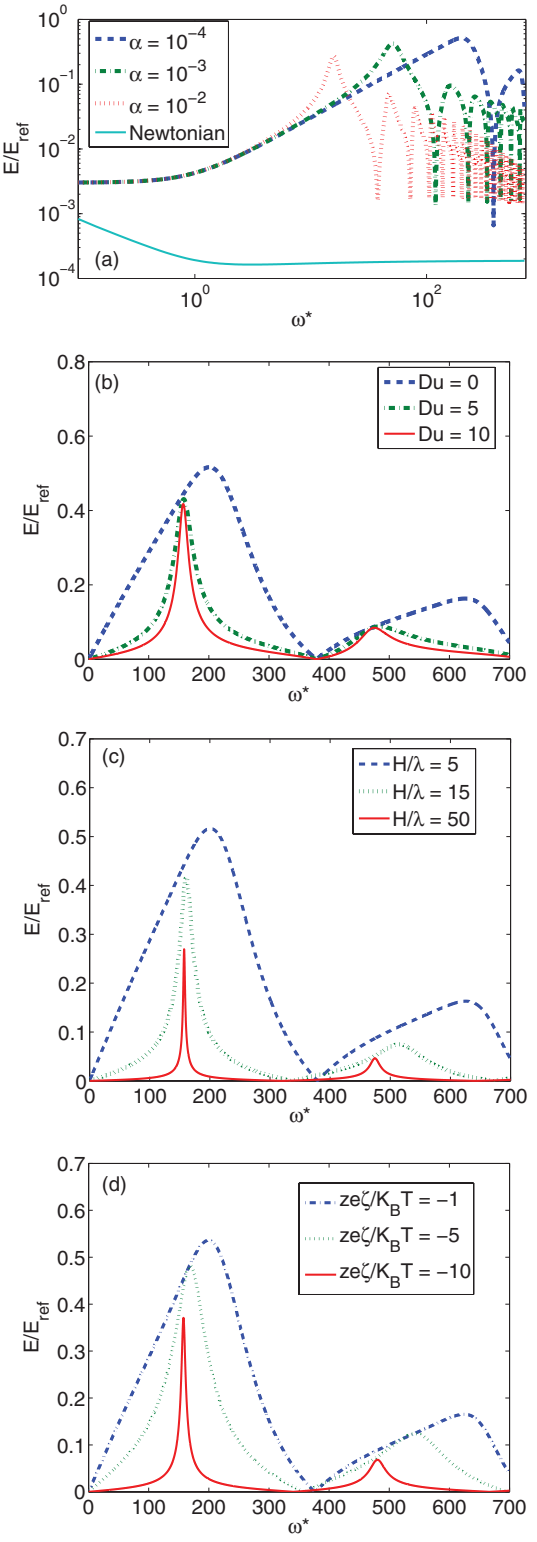

FIG. 1. (Color online) Variation of the dimensionless induced streaming potential field ($\bar{E}$) as a function of dimensionless frequency (ω^*), for (a) different values of the inverse of Deborah numbers (other parameters are Du $= 0$, $\bar{\zeta} = -1$, and $H/\lambda = 5$); (b) different Dukhin numbers (Du) (other parameters are $H/\lambda = 5$, $\bar{\zeta} = -1$, and $\alpha = 10^{-4}$); (c) different channel width to Debye length ratios (H/λ) (other parameters are Du $= 0$, $\bar{\zeta} = -1$, and $\alpha = 10^{-4}$); and (d) different dimensionless zeta potentials (other parameters are Du $= 0$, $H/\lambda = 5$, and $\alpha = 10^{-4}$).

field. Interestingly, in addition, the presence of streaming potential effects can be considered as a source of dissipation in an elastic system. Accordingly, for a more dissipative system (characterized by lower values of H/λ), we realize resonance at a higher frequency as compared to that in a less dissipative system.

Figure 1(d) depicts the variation of dimensionless induced streaming potential field ($\bar{E}$) as a function of the dimensionless frequency (ω^*), for different dimensionless values of the zeta potential. As the magnitude of $\bar{\zeta}$ increases, it is seen that the contribution of the pressure gradient term, i.e., I_1, increases. However, the contribution of the electrical term to the streaming current, i.e., I_2, increases by a larger extent. Thus from Eq. (13) it is seen that the magnitude of the induced streaming potential field decreases, as attributable to a relatively large enhancement in contribution from the electrical term. As a consequence, for higher magnitudes of zeta potential, we obtain a lower strength of the induced electrical field at the resonant frequencies.

Having looked into the streaming potential characteristics, we next attempt to address the following question: "How do electrokinetic effects influence the dynamical response of the fluidic system ?". In an effort to do so, we compare dynamic permeability characteristics in the presence and in the absence of interfacial electrokinetic interactions. Figure 2(a) depicts the variation of the dimensionless dynamic permeability (K^*) as a function of dimensionless frequency (ω^*), for different values of α. Physically the dynamic permeability is a measure of the volume flow rate for a given cross section. It can be seen that typically for low values of α (higher relaxation time), we may potentially get dramatic augmentations in the dynamic permeability at resonant frequencies, neglecting electrokinetic interactions. However, the presence of interfacial electrokinetic effects leads to an effective attenuation of the dynamic permeability at these resonating frequencies. We observe that this attenuation is more severe as the value of α is progressively reduced. We also observe that the first occurrence of resonance shifts to a higher frequency zone as the relaxation time increases (signifying lower values of α). A larger relaxation time is effectively an indicator of more prominent deviation from Newtonian behavior, with augmented elastic nature of the fluidic system, thereby implying a larger resonating frequency. In contrast to this, as the relaxation time decreases (large values of α), it can be clearly seen that the dissipative characteristics of the system appear to be significantly more prominent, so that the value of the dynamic permeability at the resonant frequency decreases and the resonating frequency shifts to the low frequency limits. In the limit as the fluid becomes Newtonian, there are no resonance peaks and the behavior is completely dissipative. Importantly, an induced streaming field leads the establishment of a resistive back electromotive forcing parameter, leading to augmented dissipative characteristics of the system, over and above the intrinsic constitutive resistive behavior of the fluid as attributable to its viscous nature. This is primarily influenced by the occurrence of the conduction current being transported through the bulk fluid. Such enhanced dissipative characteristics of the system tend to dampen out amplifications in the dynamical response to a considerable extent, typically at resonating frequencies (at which the streaming potential also attains its peak strength),

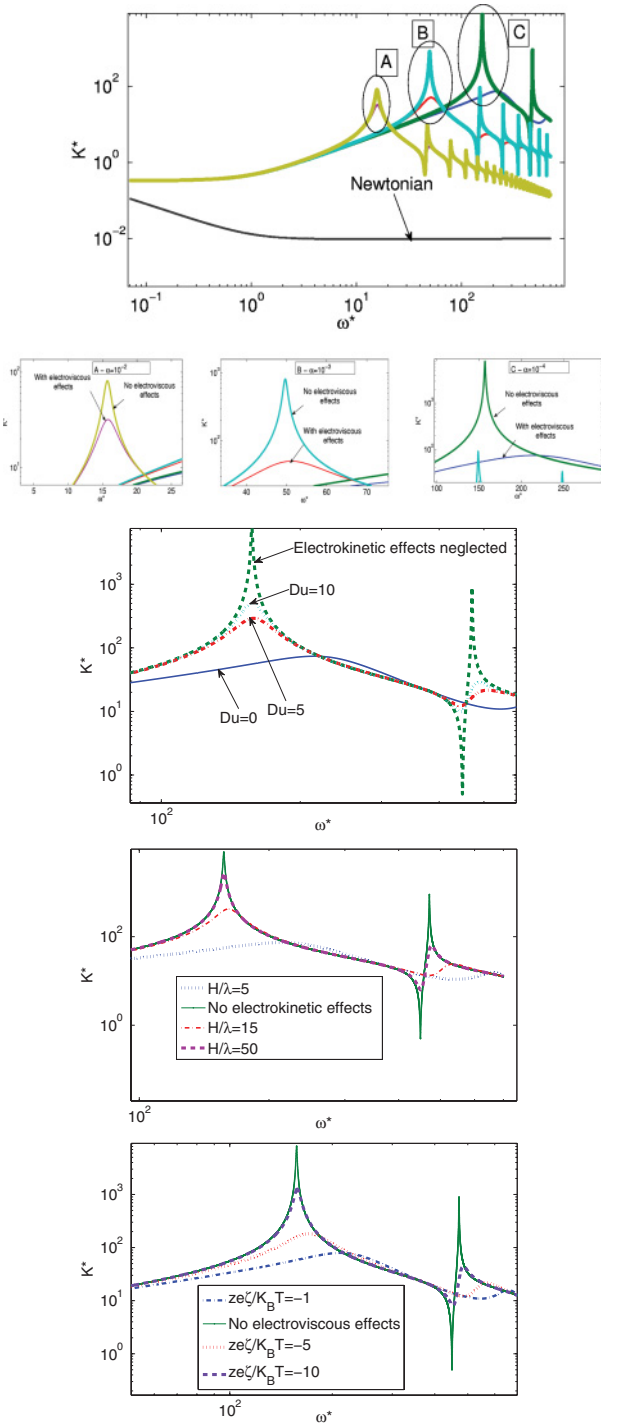

FIG. 2. (Color online) (a)–(d) Variation of the dimensionless induced streaming potential field ($\bar{E}$) as a function of dimensionless frequency (ω^*), for (a) different values of the inverse of Deborah numbers (other parameters are Du $= 0$, $\bar{\zeta} = -1$, and $H/\lambda = 5$); insets A, B, and C show magnified portions of the first resonant peaks for different inverse Deborah numbers; (b) different Dukhin numbers (Du) (other parameters are $H/\lambda = 5$, $\bar{\zeta} = -1$, and $\alpha = 10^{-4}$); (c) different channel width to Debye length ratios (H/λ) (other parameters are Du $= 0$, $\bar{\zeta} = -1$, and $\alpha = 10^{-4}$); (d) different dimensionless ζ potentials (other parameters are Du $= 0$, $H/\lambda = 5$, and $\alpha = 10^{-4}$). The dynamic permeabilities are compared for the cases in which the electrokinetic effects are neglected with the cases in which electrokinetic effects are taken into account.

so that an otherwise dramatic augmentation in the dynamic permeability value at the resonating frequency gets dampened out to a considerable extent.

Figure 2(b) depicts the variation of the dimensionless dynamic permeability (K^*) as a function of dimensionless frequency (ω^*), for different values of the Dukhin number (signifying the relative magnitude of Stern layer conductivity with respect to bulk conductivity). As discussed in the context of Fig. 1(b), the Stern layer conductivity acts so as to oppose the establishment of a large streaming potential gradient, so that additional dissipative effects in the fluidic system due to electrokinetic interactions tend to get arrested to a noticeable extent. Thus, the least net amplification in the dynamic permeability at resonance is seen when the Stern layer does not conduct. It is important to reiterate in this context that the lack of Stern layer conductivity represents the case in which the streaming current is entirely balanced out by the conduction current through the bulk. As the Stern layer conductivity increases, the contribution of electrokinetic interactions to the velocity field decreases, due to attenuation in the induced electric field. This leads to shifting of the resonating frequencies nearer to the resonating point corresponding to the case in which electrokinetic effects are neglected.

Figure 2(c) depicts the variation of the dimensionless dynamic permeability (K^*) as a function of dimensionless frequency (ω^*), for different values of H/λ. It can be seen that for larger H/λ, we obtain dynamic permeability characteristics that are reminiscent of the situation in which electrokinetic effects are neglected. For smaller H/λ ratios, on the other hand, more significant electrokinetic effects are felt [please see Fig. 1(c) along with its explanation], as attributable to more prominent protrusion of interfacial electrochemical effects (manifested in terms of differences in number densities between the counterions and the coions) into the bulk as a consequence of relatively thicker EDLs. Accordingly, channels with lower H/λ ratios are inherently more electrodissipative, resulting in stronger attenuations in the augmentation in the dynamic permeability at resonance. In addition, the frequency at which this resonating phenomenon occurs tends to shift to the higher side of the resonance frequency, reminiscent of the case in which electrokinetic effects are neglected.

Figure 2(d) depicts the variation of the dimensionless dynamic permeability (K^*) as a function of dimensionless frequency (ω^*), for different dimensionless zeta potentials ($\bar{\zeta}$). From Fig. 1(d) it can be seen the dimensionless streaming potential field decreases as the $\bar{\zeta}$ increases. Physically, the dimensionless permeability is related to the volume flow rate for a given cross section. When the amplification in the induced potential field decreases, it directly affects the velocity field in the sense that the contribution of the electroresistive component to the velocity field weakens. As a result the enhanced viscosity attributable due to the conduction current also decreases; which ultimately leads to a larger dynamic permeability.

Figure 3 depicts the variation in the maximum value of the dynamic permeability ($K^*_{\max}$) and the frequency at which the maxima occurs ($\omega^*_{\max}$) as a function of inverse Deborah number (α), for the cases where electrokinetic effects are neglected as well as for the cases in which electrokinetic effects are taken into account. It may be inferred that when the relaxation time of the fluid is large (smaller value of α), perceptible amplification in the dynamic permeability occurs at resonance, in case electrokinetic effects are negligible. The extent of this amplification drops down gradually as we move toward a higher value of α. Electrokinetic interactions, however, tend to attenuate the amplification in the dynamic permeability, for reasons as mentioned earlier. Further, the resonating frequency shifts toward higher values on consideration of interfacial electrokinetic interactions, which appears to be a progressively prominent feature as the relaxation time of the fluid increases. However, interestingly, as the relaxation time decreases, the resonances for both cases tend to occur at nearly the same frequency. In addition, we observe that as the relaxation time decreases further, there is a critical inverse Deborah number (α_{cr}) beyond which the behavior at resonance becomes fully dissipative (i.e., $K^* < 1$). The characteristics for different H/λ, Du, and $\bar{\zeta}$ follow similar trends, and are not presented here for brevity.

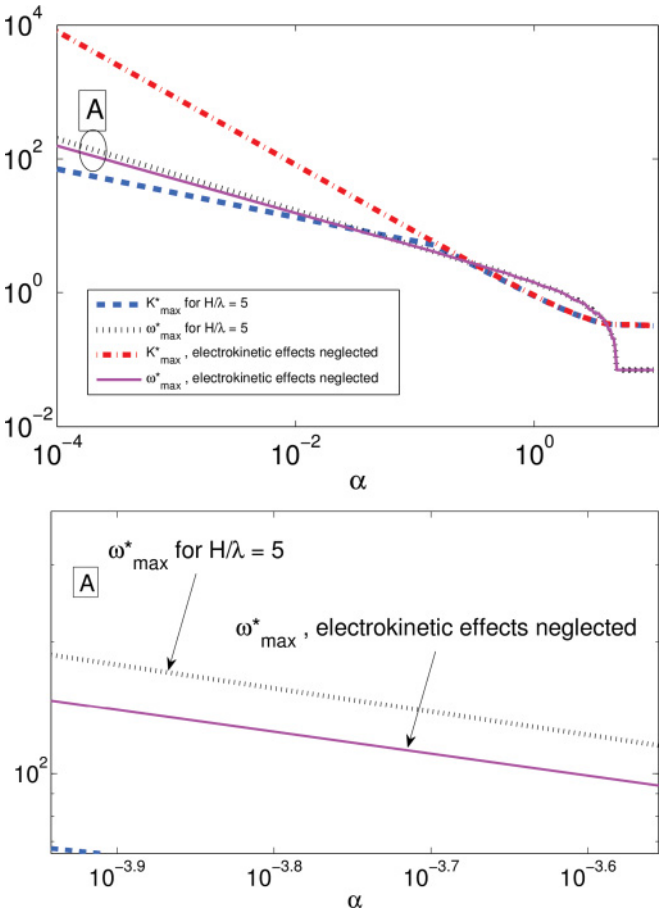

FIG. 3. (Color online) Variation in the maximum value of the dynamic permeability ($K^*_{\max}$) and the frequency at which the maximum of the dynamic permeability occurs ($\omega^*_{\max}$), as a function of the inverse Deborah number (α) for the cases in which electrokinetic effects are neglected and in which the electrokinetic effects are taken into account. Other parameters are $\bar{\zeta} = -1$, Du $= 0$, and $H/\lambda = 5$. The magnified portion A (see the bottom panel) shows the variation in the frequency at which the maxima in dynamic permeability occurs.

IV. POSSIBLE CONNECTIONS WITH EXPERIMENTS AND PRACTICAL CONSIDERATIONS

It may be stated here that the primary aim of the present work is to extend the electrokinetics-independent theoretical considerations on the dynamic permeability of viscoelastic fluids, as reported by previous researchers [4], by taking into account electrokinetic effects pertinent to narrow fluidic confinements, under the influence of EDL phenomena. In that perspective, the scope of the present paper is purely theoretical in nature, with a vision of obtaining analytical solutions to depict the role of streaming potential toward dictating the dynamic permeability of viscoelastic fluids in a microconfined environment. Having said that, we have also looked into relevant literature on experimental studies on the dynamic permeability of viscoelastic fluids. However, the experiments that have been reported in this context so far have been executed in conduit with characteristic length scales over which electrokinetic effects are not important (for example, see Refs. [53,54]). Hence, the experimental studies reported in the literature so far do not represent scalewise appropriate frameworks for testing the significance of the present findings, although the validity of the present solution is reflected from its analytical nature by itself.

Despite the nonexistence of any reported experimental study that might have acted as a basis toward assessing the predictive capabilities of our work, theoretical findings from the present study may act as precursors to new experiments that may be conducted to probe the implications of electrokinetic effects toward altering the dynamic permeability of viscoelastic fluids in narrow confinements. The concerned experimental setup may be designed by following the study of Castrejón-Pita *et al*. [53], in which the oscillating movement required to have a time-periodic pressure gradient is realized with a piston-cylinder arrangement that is driven by a motor of variable frequency. Alternatively, peristaltic pumps that are typical to several microfluidic applications may be employed for that purpose. The characteristic length scale of the fluidic channel may be designed to be in the tune of a few micrometers, so that EDL effects may turn out to be significant. Viscoelastic fluids such as cetyltrimethylammonium bromide (CTAB), which are known to ionize silica (thus leading to the formation of EDL; see [54]), may be employed as working fluids for this purpose. The electrochemical and rheological characteristics of this solution may be altered judiciously by adding different amounts of sodium salicylate (NaSal). With such a system, widely varying zeta potentials may be obtained; for example, for a 15 mM CTAB solution, a variation in salt concentration from 10 to 200 mM may result in zeta potential variations from 50 mV to -10 mV, which is a considerable experimental regime [55]. The flow velocities may be obtained by using a microscopic particle image velocimetry (micro-PIV) technique, and the analytically obtained velocity variations may be compared with experimentally obtained data. The same results may be compared with analytical solutions that are obtained without any electrokinetic considerations, in an effort to bring out the attenuating effects of streaming potential toward arresting any dramatic amplifications in the dynamic permeability at resonant frequencies.

Various substrates have been referred to in the literature, considering the distinctive roles played by their wettability characteristics toward dictating their physicochemical interactions with the ionic solution mentioned as above. For hydrophilic substrates (such as silica), the adsorption of ionic surfactants is generally perceived to be initially triggered by electrostatic attraction between head groups and the oppositely charged surface of the substrate, followed by aggregation of surfactants around the initial adsorbates with an increase in concentration [54]. As a consequence, the surface electric field is first reduced due to charge neutralization, and subsequently reversed due to surfactant aggregation. On the other hand, for hydrophobic substrates (for example, pyrolitic graphite), a lower density adsorbed layer is oriented with surfactant tails parallel to the substrate plane [54], as triggered by a strong hydrophobic interaction between the tails and the substrate. For more details on the substrate characteristics and their interaction mechanisms with the CTAB solution, one may refer to the studies of Manne *et al*. [54].

V. CONCLUSIONS

In this study, we have illustrated the implications of interfacial interactions toward altering the dynamic responses of viscoelastic fluids in narrow confinements. A subtle aspect of such considerations lies in the fact that in many such scenarios, electrokinetic effects, originating out of spontaneous interfacial electrochemical interactions, are trivially neglected based on the consideration that no external electric field acts on the system. Our studies, however, have revealed that such electrokinetic interactions, manifested through the establishment of a streaming potential field, may alter not only the characteristics of dynamic response at the resonating frequencies, but also the values of corresponding resonating frequencies. Such alterations, in effect, are achieved by intricate interactions between the elastic and dissipative effects prevailing in the system, as realized through a viscoelatic rheology of the transported fluid and electroviscous effects intrinsic to pressure-driven transport in narrow confinements. For describing our results, we have chosen property values consistent with typical biological fluids, so as to impart practical relevance to this work in the context of biomicrofluidics. The central result from our study is the fact that substantial attenuations in otherwise portrayed dramatic amplifications in dynamic responses of viscoelastic fluids may occur at the resonating frequencies, as attributable to interfacial electrokinetic interactions. In addition, our analytical investigations have revealed that the resonating frequencies themselves are likely to shift to higher values under the influence of streaming potential. Such differences in the dynamical response characteristics with and without interfacial electrokinetic interactions, however, tend to get reduced as the rheology of the fluid approaches Newtonian behavior, characterized by short relaxation times. We have also delineated the implications of the Stern layer conductivity, channel height to Debye length ratio, and the zeta potential on the pertinent characteristics.

It is also important to mention that the practical implications of the outcome of the present investigation may be far ranging, beyond the biomicrofluidic applications portrayed earlier. For

instance, one may refer to narrow fluidic devices acting as pulsating mass flow controllers [41,56]. Their frequency-dependent mass flow rate characteristics, in effect, depend heavily on the interactions between pressure-driven flow and a back electro-osmotic flow generated due to intricate interfacial electrokinetic interactions. Erroneous overestimates in possible amplifications in dynamic responses at resonating frequencies because of neglecting interfacial electrokinetic interactions may not only embed serious anomalies in their underlying design principle, but may also lead to critical malfunctioning of the devices thus conceptualized. Inferences from the present study may act as valuable pointers in arriving at a more precise and physically consistent design basis for devices with such functionalities.

APPENDIX A: DERIVATION OF EQ. (4a)

Equation (3) is a second order nonlinear ordinary differential equation, and hence would ideally require only two boundary conditions, namely, $\psi = \zeta$ at $y = 0$ (zeta potential at the wall) and $d\psi/dy = 0$ at $y = H$ (symmetry at the centerline).

In an effort to outline the solution procedure, we first nondimensionalize Eq. (3), in the form

$$\frac{d^2\bar{\psi}}{d\bar{y}^2} = \frac{H^2}{\lambda^2}\frac{1}{\bar{\zeta}}\sinh(\bar{\psi}\bar{\zeta}),$$

where $\bar{\psi} = \psi/\zeta$, $\bar{\zeta} = ze\zeta/K_BT$, and $\bar{y} = y/H$. Multiplying both sides by $2(d\bar{\psi}/d\bar{y})$, rescaling $\bar{\psi}\bar{\zeta} = \tilde{\psi}$, and integrating both sides, we get

$$\left(\frac{d\tilde{\psi}}{dy}\right)^2 = \frac{2}{(\lambda/H)^2}[\cosh(\tilde{\psi})] + C,$$

where C is an arbitrary, independent constant of integration.

In order to evaluate C, one may, in addition, consider a value of ψ at $y = H$, which we denote as ψ_c. While the choice of ψ_c can be mathematically arbitrary, the physics of EDL formation essentially implicates that ψ_c is effectively zero without EDL overlap (for details, see [13,15,35–40]). Interestingly, from a pure mathematical perspective, it has also been discussed by Berg and Ladipo [35] that "this third condition does not lead to an overdetermined problem." As such, the problem posed is gauge invariant and this kind of choice is possible because one can write

$$n_0 \exp\left(\frac{-ze\psi}{K_BT}\right) = n_0 \exp\left(\frac{-ze\psi_c}{K_BT}\right)\exp\left(\frac{-ze\,(\psi-\psi_c)}{K_BT}\right) = n_0^* \exp\left(\frac{-ze\,(\psi-\psi_c)}{K_BT}\right),$$

say, where $n_0^* = n_0 \exp(-ze\psi_c/K_BT)$. Following Berg and Ladipo [35], it may further be mentioned that one way of interpreting the situation is to consider n_0 to be an eigenvalue of the nonlinear Poisson-Boltzmann equation, subject to the two fundamental boundary conditions and an additional constraint on the centerline potential (without EDL overlap, the centerline behaves like a "far stream" that does not feel the charging effect of the wall, so that $\psi_c = 0$). It may further be mentioned in this context that under overlapped EDL conditions, the value of ψ_c may turn out to be nonzero, but the same can be specified from further constraints on the electrochemical reaction equilibria involved—there is a large volume of literature on this aspect, but we simply do not address those considerations here because our study does not address the cases with EDL overlap.

With the above considerations for determining the constant of integration C, it follows that $C = -2[\cosh(\tilde{\psi}_c)/(\lambda/H)^2]$, so that one may write

$$\left(\frac{d\tilde{\psi}}{dy}\right)^2 = \left(\frac{2\,\sinh(\tilde{\psi}/2)}{(\lambda/H)}\right)^2 - \left(\frac{2\,\sinh(\tilde{\psi}_c/2)}{(\lambda/H)}\right)^2.$$

Considering the case without involving EDL overlap ($\psi_c = 0$), it follows from the above that

$$\left(\frac{d\tilde{\psi}}{dy}\right) = -\left(\frac{2\sinh(\tilde{\psi}/2)}{(\lambda/H)}\right).$$

Notably, the negative square root has been taken here to accommodate the fact that the EDL potential decays to zero away from the wall. Separating variables in the above and setting $\tanh(\tilde{\psi}/4) = \alpha$, one gets

$$\frac{d\alpha}{\alpha} = -\frac{d\bar{y}}{\lambda/H}.$$

Integrating the above, it follows that

$$\ln\left(\frac{\tanh(\tilde{\psi}/4)}{\tanh(\tilde{\psi}_{\bar{y}=0}/4)}\right) = -\frac{\bar{y}}{\lambda/H},$$

so that

$$\tanh(\bar{\psi}\bar{\zeta}/4) = \tanh(\bar{\zeta}/4)\exp\left(\frac{-y}{\lambda/H}\right).$$

Notably, the above solution [Eq. (4a) in our paper] is identical to Eq. (8.58) of the seminal textbook of Bruus [40].

APPENDIX B: DERIVATION OF EQ. (9a)

The governing differential equation for the velocity field reads [please see Eq. (8)]

$$\frac{d^2U}{dy^2} + U\left(\frac{i\rho\omega + \rho\omega^2 t_m}{\eta}\right) = \frac{1}{\eta}\frac{\partial P}{\partial x}(1 - i\omega t_m) + \frac{\varepsilon\tilde{E}\zeta}{\eta\lambda^2/H^2}\frac{\sinh(\bar{\psi}\bar{\zeta})}{\bar{\zeta}}(1 - i\omega t_m).$$

Introducing the following dimensionless parameters: $\bar{y} = y/H$, $\omega^* = \omega t_m$, $\beta^2 = \rho(\omega^{*2} + i\omega^*)/\eta t_m$, $U^* = U/(\partial P/\partial x)H^2/\eta$, $\bar{E} = \tilde{E}/(\partial P/\partial x)H^2/\varepsilon\zeta$, $\bar{\omega} = i\omega t_m + \omega^2 t_m^2$, and $\alpha = \rho H^2/\eta t_m$, we obtain

$$\frac{d^2U^*}{d\bar{y}^2} + U^*\beta^2H^2 = (1 - i\omega t_m) + \bar{E}\frac{\sinh(\bar{\psi}\bar{\zeta})}{(\lambda/H)^2\bar{\zeta}}(1 - i\omega t_m).$$

For the dimensionless pressure term, i.e., the first term on the right-hand side, the particular integral is given by

$$\frac{1 - i\omega^*}{\beta^2H^2}.$$

For the electrical term (the second term in the right-hand side), the particular integral is found out using the variation of parameter method. The particular integral can be written in the form of

$$U_p^* = a_1u_1 + a_2u_2,$$

where $u_1 = \cos(\beta H \bar{y})$, $u_2 = \sin(\beta H \bar{y})$, and

$$U_p^* = a_1 \cos(\beta H \bar{y}) + a_2 \sin(\beta H \bar{y}).$$

The Wronksian for this system is

$$W = \begin{vmatrix} u_1 & u_2 \\ u_1' & u_2' \end{vmatrix} = \begin{vmatrix} \cos(\beta H \bar{y}) & \sin(\beta H \bar{y}) \\ -\beta H \sin(\beta H \bar{y}) & \beta H \cos(\beta H \bar{y}) \end{vmatrix} = (\beta H).$$

The unknown parameters are given by

$$a_1 = \int_0^{\bar{y}} \frac{-f}{W} u_2 \, d\bar{y}; \qquad a_2 = \int_0^{\bar{y}} \frac{f}{W} u_1 \, d\bar{y},$$

where

$$f = \bar{E} \frac{1 - i\omega t_m}{\frac{\lambda^2}{H^2}\bar{\zeta}} \sinh(\bar{\psi}\bar{\zeta}).$$

Thus we obtain

$$a_1 = \int_0^{\bar{y}} -\bar{E} \frac{1 - i\omega t_m}{\beta H \frac{\lambda^2}{H^2}\bar{\zeta}} \sinh(\bar{\psi}\bar{\zeta}) \sin(\beta H \bar{y}) d\bar{y},$$

$$a_2 = \int_0^{\bar{y}} \bar{E} \frac{1 - i\omega t_m}{\beta H \frac{\lambda^2}{H^2}\bar{\zeta}} \sinh(\bar{\psi}\bar{\zeta}) \cos(\beta H \bar{y}) d\bar{y}.$$

Hence the solution can be written as

$$U^* = C_1 \cos(\beta H \bar{y}) + C_2 \sin(\beta H \bar{y}) + \frac{1 - i\omega t_m}{\beta^2 H^2} + \bar{E} \frac{1 - i\omega t_m}{\beta H \frac{\lambda^2}{H^2}\bar{\zeta}} \left[-\cos(\beta H \bar{y}) \int_0^{\bar{y}} \sinh(\bar{\psi}\bar{\zeta}) \sin(\beta H \bar{y}) d\bar{y} + \sin(\beta H \bar{y}) \int_0^{\bar{y}} \sinh(\bar{\psi}\bar{\zeta}) \cos(\beta H \bar{y}) d\bar{y} \right].$$

Enforcing the no slip boundary condition at the wall, i.e., $y = 0$, we get

$$C_1 = -\frac{1 - i\omega t_m}{\beta^2 H^2}.$$

Enforcing the symmetry boundary condition at the wall, i.e., $dU^*/d\bar{y} = 0$, we get (noting that $\bar{\psi} = 0$ at $\bar{y} = 1$)

$$-C_1 \sin(\beta H) + C_2 \cos(\beta H) + \bar{E} \frac{1 - i\omega t_m}{\beta H \frac{\lambda^2}{H^2}\bar{\zeta}} \left[\sin(\beta H) \int_0^1 \sinh(\bar{\psi}\bar{\zeta}) \sin(\beta H \bar{y}) d\bar{y} + \cos(\beta H) \int_0^1 \sinh(\bar{\psi}\bar{\zeta}) \cos(\beta H \bar{y}) d\bar{y} \right] = 0,$$

$$C_2 = C_1 \frac{\sin(\beta H)}{\cos(\beta H)} + \bar{E} \frac{1 - i\omega t_m}{\beta H \frac{\lambda^2}{H^2}\bar{\zeta}} \left[-\tan(\beta H) \int_0^1 \sinh(\bar{\psi}\bar{\zeta}) \sin(\beta H \bar{y}) d\bar{y} - \int_0^1 \sinh(\bar{\psi}\bar{\zeta}) \cos(\beta H \bar{y}) d\bar{y} \right].$$

Thus the velocity profile obtained on substitution of the respective constants is given by

$$U^* = \left(\frac{1 - i\omega^*}{\alpha\bar{\omega}} \right) \left(1 - \frac{\cos[\sqrt{\alpha\bar{\omega}}(1 - \bar{y})]}{\cos(\sqrt{\alpha\bar{\omega}})} \right) + \bar{E} \frac{1 - i\omega^*}{\bar{\zeta} \left(\frac{\lambda}{H}\right)^2 \sqrt{\alpha\bar{\omega}}} \left[-\cos(\sqrt{\alpha\bar{\omega}}\bar{y}) \int_0^{\bar{y}} \sinh(\bar{\psi}\bar{\zeta}) \sin(\sqrt{\alpha\bar{\omega}}\bar{y}) d\bar{y} + \sin(\sqrt{\alpha\bar{\omega}}\bar{y}) \int_0^{\bar{y}} \sinh(\bar{\psi}\bar{\zeta}) \cos(\sqrt{\alpha\bar{\omega}}\bar{y}) d\bar{y} - \sin(\sqrt{\alpha\bar{\omega}}\bar{y}) \tan(\sqrt{\alpha\bar{\omega}}) \int_0^1 \sinh(\bar{\psi}\bar{\zeta}) \sin(\sqrt{\alpha\bar{\omega}}\bar{y}) d\bar{y} - \sin(\sqrt{\alpha\bar{\omega}}\bar{y}) \int_0^1 \sinh(\bar{\psi}\bar{\zeta}) \cos(\sqrt{\alpha\bar{\omega}}\bar{y}) d\bar{y} \right].$$

[1] K. Warner and J. R. Beamish, Phys. Rev. B **50**, 15896 (1994).
[2] D. Tsiklauri and I. Beresnev, Phys. Rev. E **63**, 046304 (2001).
[3] M. L. Haro, J. A. P. Río, and S. Whitaker, Transp. Porous Media **25**, 167 (1996).
[4] J. A. del Río, M. L. de Haro, and S. Whitaker, Phys. Rev. E **58**, 6323 (1998).
[5] Y. Achdou and M. Avellaneda, Phys. Fluids A **4**, 2651 (1992).
[6] M. Avellaneda and S. Torquato, Phys. Fluids A **3**, 2529 (1991).
[7] L. Casanellas and J. Ortín, J. Non-Newtonian Fluid Mech. **166**, 1315 (2011).
[8] M. Sahimi, Rev. Mod. Phys. **65**, 1393 (1993).
[9] M. Castro, M. E. Bravo-Gutiérrez, A. Hernández-Machado, and E. C. Poiré, Phys. Rev. Lett. **101**, 224501 (2008).
[10] D. Lafarge, Phys. Fluids A **5**, 500 (1993).
[11] J. Flores, E. Corvera Poiré, J. A. del Río, and M. López de Haro, J. Theor. Biol. **265**, 599 (2010).
[12] S. Cuevas and J. A. del Río, Phys. Rev. E **64**, 016313 (2001).
[13] R. J. Hunter, *Zeta Potential in Colloid Science* (Academic, New York, 1981).
[14] R. F. Probstein, in *Physicochemical Hydrodynamics: An Introduction* (Wiley, New York, 1994), p. 400.
[15] S. Ghosal, Annu. Rev. Fluid Mech. **38**, 309 (2006).
[16] V. Ajaev, *Interfacial Fluid Mechanics* (Springer, New York, 2012).
[17] A. M. Afonso, M. A. Alves, and F. T. Pinho, J. Non-Newtonian Fluid Mech. **159**, 50 (2009).

[18] C. L. A. Berli and M. L. Olivares, J. Colloid Interface Sci. **320**, 582 (2008).
[19] S. Das and S. Chakraborty, Anal. Chim. Acta **559**, 15 (2006).
[20] S. Dhinakaran, A. M. Afonso, M. L. Alves, and F. T. Pinho, J. Colloid Interface Sci. **344**, 513 (2010).
[21] D. I. Graham and T. E. R. Jones, J. Non-Newtonian Fluid Mech. **54**, 465 (1994).
[22] M. Hadigol, R. Nosrati, and M. Raisee, Colloids Surf. A **374**, 142 (2011).
[23] M. L. Olivares, L. Vera-Candioti, and C. L. A. Berli, Electrophoresis **30**, 921 (2009).
[24] H. M. Park and W. M. Lee, Lab Chip **8**, 1163 (2008).
[25] N. Vasu and S. De, Int. J. Eng. Sci. **48**, 1641 (2010).
[26] C. Zhao and C. Yang, Electrophoresis **31**, 973 (2010).
[27] C. Zhao and C. Yang, Int. J. Emerg. Mult. Fluid Sci. **1**, 37 (2009).
[28] C. Zhao, E. Zholkovskij, J. Masliyah, and C. Yang, J. Colloid Interface Sci. **326**, 503 (2008).
[29] W. B. Zimmerman, J. M. Rees, and T. J. Craven, Microfluid. Nanofluid. **2**, 481 (2006).
[30] G. H. Tang, X. F. Li, Y. L. He, and W. Q. Tao, J. Non-Newtonian Fluid Mech. **157**, 133 (2009).
[31] M. B. Akgul and M. Pakdemirli, Int. J. Nonlinear Mech. **43**, 985 (2008).
[32] C. Zhao and C. Yang, Appl. Math. Comput. **211**, 502 (2009).
[33] J. E. Gomez and G. B. Thurston, Biorheology **30**, 409 (1993).
[34] M. K. Sharp, G. B. Thurston, and J. E. Moore, Biorheology **33**, 185 (1996).
[35] P. Berg and K. Ladipo, Proc. R. Soc. London, Ser. A **465**, 2663 (2009).
[36] P. Dutta and A. Beskok, Anal. Chem. **73**, 5097 (2001).
[37] A. L. Garcia, L. K. Ista, D. N. Petsev, M. J. O'Brien, P. Bisong, A. A. Mammoli, S. R. J. Brueck, and G. P. López, Lab Chip **5**, 1271 (2005).
[38] R. J. Hunter and L. R. White, *Foundations of Colloid Science* (Clarendon, Oxford, 1989).
[39] H. Ohshima, *Theory of Colloid and Interfacial Electric Phenomena* (Elsevier/Academic Press, Amsterdam, 2006).
[40] H. Bruus, in *Theoretical Microfluidics* (Oxford University Press, New York, 2008), p. 153.
[41] J. Chakraborty, S. Ray, and S. Chakraborty, Electrophoresis **33**, 419 (2012).
[42] A. Bandopadhyay and S. Chakraborty, Langmuir **27**, 12243 (2011).
[43] J. Chakraborty and S. Chakraborty, Phys. Fluids **23**, 082004 (2011).
[44] J. Chakraborty and S. Chakraborty, Phys. Fluids **22**, 122002 (2010).
[45] P. Goswami and S. Chakraborty, Langmuir **26**, 581 (2010).
[46] F. Munshi and S. Chakraborty, Phys. Fluids **21**, 122003 (2009).
[47] S. Das and S. Chakraborty, Langmuir **25**, 9863 (2009).
[48] T. Das, S. Das, and S. Chakraborty, J. Chem. Phys. **130**, 244904 (2009).
[49] S. Chakraborty and S. Das, Phys. Rev. E **77**, 037303 (2008).
[50] L. Gary Leal, *Advanced Transport Phenomena* (Cambridge University Press, Cambridge, England, 2007).
[51] R. B. Bird, W. E. Stewart, and E. N. Lightfoot, *Transport Phenomena* (Wiley, New York, 1960).
[52] C. Davidson and X. Xuan, Electrophoresis **29**, 1125 (2008).
[53] J. R. Castrejón-Pita, J. A. del Río, A. A. Castrejón-Pita, and G. Huelsz, Phys. Rev. E **68**, 046301 (2003).
[54] S. Manne, J. Cleveland, H. Gaub, G. Stucky, and P. Hansma, Langmuir **10**, 4409 (1994).
[55] A. Shukla and H. Rehage, Langmuir **24**, 8507 (2008).
[56] S. Chakraborty and S. Ray, Phys. Fluids **20**, 083602 (2008).